The Role of Phenylalanine 31 in Maintaining the Conformational Stability of Ribonuclease P2 from *Sulfolobus solfataricus* under Extreme Conditions of Temperature and Pressure†

Enrico Mombelli,‡,§ Mohammad Afshar,|| Paola Fusi,§ Margherita Mariani,§ Paolo Tortora,§ James P. Connelly,‡ and Reinhard Lange*,‡

INSERM U128, BP 5051, 34033 Montpellier, France, Dipartimento di Fisiologia e Biochimica generali, Università degli Studi di Milano, via Celoria 26, 20133 Milano, Italy, and Protein Structure Group, Department of Chemistry, University of York, York YO1 5DD, U.K.

Received February 28, 1997; Revised Manuscript Received May 12, 1997⊗

ABSTRACT: Ribonuclease P2 from the thermophilic archaebacterium *Sulfolobus solfataricus* is a small protein (7 kDa) with a known three-dimensional structure. Inspection of the structure and molecular dynamics simulation reveal that three aromatic residues (Phe5, Phe31, and Tyr33) from the hydrophobic core have a strong van der Waals interaction energy. We studied the thermodynamics of the heat, cold, and pressure-induced protein conformational changes of the wild type and of the F31A and F31Y mutants by analyzing the protein UV absorbance in the fourth derivative mode. The wild-type protein was extremely stable under all conditions of temperature and pressure. Heat and cold denaturation of both mutants, as well as denaturation by pressure of the F31A mutant, led to significant blue shifts of the derivative spectrum, indicating increased solvent exposure of Tyr33. For the F31Y mutant, high pressure (400 MPa) protected the protein against thermal denaturation. This study, probing the properties of the hydrophobic aromatic core, complements a thermal unfolding study which probes the overall structural changes [Knapp, S., Karshikoff, A., Berndt, K. D., Christova, P., Atanasov, B., & Ladenstein, R. (1996) *J. Mol. Biol. 264,* 1132−1144]. The differences observed in response to extremes of temperature, pressure, and pH may be rationalized by an unfolding mechanism involving larger parts of the peripheral protein while the integrity of the hydrophobic core is maintained.

Understanding the structural changes occurring in the course of protein folding and unfolding potentially provides invaluable information about the chemical interactions between particular amino acid residues and/or protein domains and the forces implied for maintaining the complex and generally unique conformation of a given protein. In turn, this information is needed for an understanding and control of enzyme activity. In recent years, there has been growing interest in the study of protein denaturation mechanisms. The current progress has been facilitated by the availability of mutant protein forms, by higher resolution detection methods, such as X-ray protein crystallography and NMR,[1] by the optimization of time-resolved spectroscopic methods, and by the adaptation of the technical setup to extreme temperature and pressure conditions. The outcome of protein denaturation studies is important for many biotechnological processes where proteins are employed under nonstandard physical−chemical conditions (Herbert, 1992). Additional interest comes from the very relevant problem of the conformational changes of prions.

Proteins have been denatured under extreme conditions of temperature, pressure, and pH, by chemicals like urea and guanidine hydrochloride, and by solvents. Yet, despite the diversity of experimental approaches, our knowledge of the laws underlying protein denaturation mechanisms is rather incomplete. Factors postulated for determining the native protein conformation are van der Waals interactions between inner core residues, local and intersegment hydrogen bonds, disulfide bonds, and salt bridges (Dill, 1990). On the other hand, the interaction of the residues located at the protein surface with the solvation shell is also a very important factor. It is established now that to a certain extent the hydrophobic inner residues become more exposed to the solvent (water) upon denaturation. In particular, aromatic amino acids have been used as intrinsic probes for protein defolding induced exposure of hydrophobic residues, as their spectroscopic properties are strongly influenced by the presence of polar water molecules. The sequence of events occurring during protein denaturation is another problem. For several model proteins, one or more intermediates [sometimes called

† Part of this work was supported by the COST D6 Action, the French−Italian GALILEE program, by the Italian Ministero dell'Università e della Ricerca Scientifica e Tecnologica (40% program), and by the Italian Consiglio Nazionale delle Ricerche. J.P.C. and M.A. were supported by an INSERM long-term fellowship (Poste vert) and a European Union HCM fellowship, respectively.

* Author to whom correspondence should be sent [telephone, +33 (0)4 67 61 33 65; Fax, +33 (0)4 67 52 36 81; e-mail, lange@xerxes.cnrs-mop.fr].

‡ INSERM U128.

§ Università degli Studi di Milano.

|| University of York.

⊗ Abstract published in *Advance ACS Abstracts,* July 1, 1997.

[1] Abbreviations: NMR, nuclear magnetic resonance; P2, ribonuclease P2 from *Sulfolobus solfataricus,* also called Sso7d; Sac7d, a DNA binding protein from *Sulfolobus acidocaldarius;* DSC, differential scanning calorimetry; CD, circular dichroism; F31A and F31Y, mutants of P2 where Phe31 is replaced by alanine or tyrosine; vdW, van der Waals; rms, root mean square; TIM, triose-phosphate isomerase; ATEE, *N*-acetyl-L-tyrosine ethyl ester.

S0006-2960(97)00467-4 CCC: $14.00

"molten globule" or "premolten globule" (Uversky & Ptitsyn, 1996)] have been found. However, the prediction of these intermediates from the native protein structure constitutes still a major challenge.

In our opinion, such complex problems can best be studied by taking proteins of unusually high stability under extreme conditions where the analysis of the mechanism of denaturation might be simplified. In that sense, thermophilic enzymes have been widely investigated because of their surprising resistance to denaturing agents compared to their mesophilic counterparts (Vieille & Zeikus, 1996, and bibliography therein). Ribonuclease P2, from *Sulfolobus solfataricus* (Fusi et al., 1993), a thermoacidophilic archaebacterium that lives at 87 °C and acidic pH in hot springs (De Rosa et al., 1984), is well suited for this type of study. This very small protein (7 kDa) is resistant to very high temperatures (Fusi et al., 1993): at neutral pH its melting temperature is near the boiling point of water (Knapp et al., 1996). The physiological function of this enzyme is not yet clear: apart from its ribonuclease function, Baumann et al. (1994) (who call that protein Sso7d) reported that it is an abundant DNA binding protein; upon binding it protects DNA from thermal denaturation. Its tertiary structure in solution, as determined by NMR (Baumann et al., 1994; Consonni et al., 1995), shows that the protein is made up of a triple-stranded β-sheet which is orthogonal to a double-stranded β-sheet, and it contains only a small α-helix at the C-terminus. It has a hydrophilic mantle which contains many basic residues (2 arginines and 13 lysines) and a strongly hydrophobic core. Recently, the protein-encoding gene has been cloned and the protein expressed in *Escherichia coli* (Fusi et al., 1995). Furthermore, the small size of this protein allowed easy construction and expression of several mutant forms. Ribonuclease P2 thus appears to be an ideal candidate to study the structural basis of protein stability.

As an intrinsic probe, we used the UV absorbance of tyrosine and tryptophan in the fourth derivative mode. This method allows enhancement of the generally poor resolution of zero-order UV absorbance spectra (Lange et al., 1996a) and is a recent development in the study of protein structural changes during thermal denaturation (Mozo Villarias et al., 1991; Laderman et al., 1993; Lange et al., 1996a,b). Application of this method to denaturation of several well characterized proteins has shown that the local environmental changes reflect the cooperative denaturation of the protein. Furthermore, in the fourth derivative mode, the wavelength position of the maximum amplitude of tyrosine can be used to evaluate the polarity of its microenvironment. In this paper we study the importance of interactions within the hydrophobic core for maintaining the protein stability. The residues belonging to this domain can be identified by calculating the solvent-accessible surface of the NMR average structure of P2. Eleven residues display over 85% buried surface and are considered to belong to the hydrophobic core: Val3, Phe5, Val14, Ile19, Val22, Ile29, Phe31, Tyr33, Val45, Ala50, and Leu54. As suggested by molecular dynamics simulation (see below), three aromatic residues show a particularly high van der Waals interaction energy: Phe5, Phe31, and Tyr33. Among these, we have studied the structural importance of Phe31. For that, we analyzed the heat, cold, and pressure denaturation profiles of the wild-type ribonuclease P2 and its mutants F31A and F31Y.

MATERIALS AND METHODS

Proteins. Ribonuclease P2 from the archaebacterium *S. solfataricus* was expressed in *E. coli* and purified as described by Fusi et al. (1995). This recombinant ribonuclease has proven to be indistinguishable from the wild-type P2 on the basis of heat stability, pH optimum of the RNase activity, and RNA digestion pattern (Fusi et al., 1995). The F31A and F31Y mutants were obtained by site-directed mutagenesis as reported by Consonni et al. (1996). In the F31A mutant Phe31 has been replaced by alanine and in the F31Y mutant by tyrosine. The three proteins were electrophoretically (silver staining) pure. The mutant enzymes were stored lyophilized at −20 °C and dissolved just before use in the buffer. The wild-type (wt) ribonuclease was dissolved in pure water at a concentration of 10 mg/mL and stored at −20 °C. Under these conditions the enzymes were indefinitely stable.

Buffers and Chemicals. MES buffer from Sigma (St. Louis, MO), dipotassium hydrogen phosphate trihydrate from Merck (Darmstadt, Germany), and tetrapotassium pyrophosphate from Carlo Erba (Milano, Italy) were used. MES buffer was used in high-pressure experiments because its p*K* does not change significantly as a function of pressure (Kitamura & Itoh, 1987). Phosphate and pyrophosphate buffers were used during thermal denaturation since their p*K* values are rather stable with respect to temperature (Fasman, 1976). Urea, ultra pure (molecular biology grade), was from Research Organics (Cleveland, OH).

UV Spectroscopy. The UV spectra were recorded with a Cary 3E (Varian) spectrophotometer which has a high-wavelength reproducibility (SD < 0.02 nm). Each spectrum (corrected for the baseline) was the result of five accumulations. The monochromator proceeded in steps of 0.1 nm with a data acquisition time of 0.3 s per step. The spectral bandwidth was 1.0 nm. In place of the sample compartment a thermostated high-pressure (0.1−500 MPa) cell was installed. The cell was an improved version of that described by Hui Bon Hoa et al. (1982). It was made of Marval X12 steel with windows of sapphire and surrounded by a steel mantle through which the thermostating fluid (water or ethanol) was pumped (Lange et al., 1996a). The sample was placed into a cylindrical quartz cuvette (volume 1.3 mL) which was closed by a Dura-Seal polyethylene stretch film. The pressure vector was water.

Experimental. In each experiment the enzyme concentration was 0.5 mg/mL with the exception of the F31A mutant in pressure denaturation experiments, where the concentration was 0.3 mg/mL. After each change of temperature or pressure the system was allowed to equilibrate for 5 min before spectral recording. For cold denaturation experiments the sample was first pressurized at 25 °C to 200 MPa, and then the temperature was decreased stepwise to −20 °C. Under these conditions the sample solution stayed in the liquid state. Water condensation and ice formation on the sapphire windows were avoided by directing a fine nitrogen gas flow over the windows.

Data Processing. The fourth derivatives of the UV spectra were evaluated with the recent optimized spectral shift method (Lange et al., 1996a) using a Sigma Plot (Jandel) based program. This method consisted of four sequential shifts of 2.5, 2.6, 2.7, and 2.6 nm, followed by their mutual spectral subtractions. A mean derivation window of 2.6 nm

was chosen as it gives optimal results (a compromise between signal to noise ratio, spectral resolution, and no spectral distortion) for tyrosine spectra around 283 nm. The resulting derivative spectrum reflects the averaged environments of the tyrosines with some small residual contribution due to the overlapping tryptophan band. A similar procedure employing a derivation window of 1.6 nm was used to optimize the tryptophan band around 287 nm. These derivative spectra were then smoothed linearly by a sliding box of 11 data points. All spectra except of those of the cold denaturation experiments, where no physical chemical data are available, were corrected for the pressure and temperature effects on the specific volume of water according to Kell (1973) and Gibson and Loeffler (1941). The polarity of the tyrosine environments in the native state at 25 °C was evaluated quantitatively in terms of a mean dielectric constant ϵ_r. This facility appeared as a result of our recent analysis of the fourth derivative spectra of *N*-acetyl-L-tyrosine ethyl ester (or ATEE; a model for tyrosine residues in proteins) as a function of solvent polarity. For solvents ranging from water to cyclohexane, a linear relationship was found between λ_m (ranging from 282.0 to 287.7 nm) and the dielectric constant of the solvent (Lange et al., 1996a,c). With temperature, the value of the dielectric constant of water varies, and at temperatures other than 25 °C, the environment of the tyrosine was judged by the λ_m position relative to the corresponding λ_m for aqueous ATEE. The maximum absorption wavelength of ATEE shifts in a linear manner to the red from 282.0 nm at 5 °C to 282.9 nm at 90 °C. Under cold denaturation conditions at 200 Mpa, ATEE λ_m shifts to the blue from 282.2 nm at 25 °C to 281.9 nm at −20 °C. Pressure up to 450 Mpa does not shift the ATEE λ_m significantly.

Thermodynamics. The thermodynamic parameters ΔG, ΔH, ΔS, and ΔV of the pressure- and temperature-induced spectral transitions were determined by analyzing the fourth derivative spectra at characteristic wavelengths, where the magnitude, A, of the transition had a maximum. With very few exceptions (see later) all transitions were reversible and had sigmoidal character. We used a simple two-state model,

$$K = \frac{A - A_n}{A_d - A} = \frac{d}{n} \quad (1)$$

where K is the equilibrium constant between the denatured (d) and the native (n) protein conformational states which are characterized by the spectral amplitudes A_d and A_n. Introducing thermodynamic relationships, eq 1 transforms to

$$A = \frac{A_n - A_d}{1 + e^{-[(\Delta G_{p=0} + p\Delta V)/RT]}} + A_d \quad (2)$$

and

$$A = \frac{A_n - A_d}{1 + e^{-[(\Delta H - T\Delta S)/RT]}} + A_d \quad (3)$$

for the pressure and temperature denaturation, respectively. The fit of $A = f(p)$ and $A = f(1/T)$ in eqs 2 and 3 permitted then the determination of the thermodynamic parameters.

Molecular Dynamics Simulation. To gain insight into the molecular basis of the structural stability of the wild-type P2, a molecular dynamics study was carried out using the stochastic boundary methodology with explicit solvent. The methodology has been previously described in detail (Brooks & Karplus, 1989; Caflisch & Karplus, 1995). Briefly, the calculations were performed with the molecular mechanics package CHARMM (Brooks et al., 1983), version 25a1. The polar hydrogen topology was used, along with the PARM22 parameter and AMINO22 topology set. For the water molecules the TIP3 model was employed (Jorgensen et al., 1983). For the electrostatic term of the potential, a constant dielectric of 1 was used. The van der Waals (vdW) term was calculated using the standard CHARMM Lennard-Jones 6−12 potential. Nonbonded interactions were maintained in a list up to a cutoff distance of 10 Å. A shift function was applied to the electrostatic term and switch to the vdW interaction between 9.0 and 8.0 Å.

Coordinates for NMR solution structure of P2 were taken from the Protein Data Bank (Bernstein et al., 1977; reference 1SSO). Polar hydrogens were added using CHARMM HBUILD, and the structure was energy minimized using constrained ABNR minimization for 400 steps (tight on backbone, looser on side chains). After solvation and solvent equilibration, the system was further energy minimized using 100 SD steps. The P2 structure (620 atoms) was centered in a sphere of 30 Å radius consisting of 3296 water molecules (total of 10 508 atoms). A deformable boundary potential and a temperature bath coupling parameter of 5 ps were used. Temperature was initially set at 240 K and then increased to 300 K during 20 ps. The simulation was carried on for a further 430 ps, using SHAKE. A time step of 1 fs was used with the Langevin algorithm. Coordinates and full-energy terms were saved every 0.5 ps. The calculations required 280 h of CPU time on an SGI R10000 computer.

RESULTS

Wild-Type Ribonuclease P2. The wild-type form proved to be extremely stable to temperature, pressure, and pH. The fourth derivative UV spectra were unaffected between pH 9 and pH 3 by temperatures between room temperature and 90 °C. At pH 1, irreversible spectral changes (an additional band in the 300 nm region) occurred at temperatures above 40 °C. We do not know the origin of this band, but since its occurrence was irreversible, we did not study this transition further. In the presence of 6 M urea it was stable at pH 7.4 up to 60 °C. Under pressure, it was also stable up to the limits of our experimental setup, i.e., 500 MPa between pH 9 and pH 3 and up to 200 MPa at pH 1. The only reversible spectral transition was obtained in a cold denaturation experiment at pH 7.4 in the presence of 4 M urea, where the λ_{max} of the derivative spectrum was shifted from 283.8 to 283.3 nm (see Figure 3B), a larger shift than expected for ATEE under identical conditions, suggesting that the protein tyrosine environment is becoming more exposed. However, this transition took place only below −10 °C, and it was not possible to measure its end point. Nevertheless, by imposing the same transition amplitude as that obtained with the F31A mutant, the thermodynamic parameters could be evaluated as $\Delta H = -102$ kJ/mol and $\Delta S = -408$ J/(mol·K) (see Table 1).

The F31A Mutant. In contrast to the very stable wild-type P2, the UV spectrum of the F31A mutant was much more sensitive to changes in temperature and pressure. These

Table 1: Heat and Cold Denaturation of Ribonuclease P2[a]

protein	denaturant	ΔH (kJ/mol)	ΔS [J/(mol·K)]	T_m (°C)	λ_{max} (nm) native	λ_{max} (nm) denatured
wild type	cold (in 4 M urea)	-102 ± 13	-408 ± 52	-20	283.8	283.3
F31A	heat	170 ± 32	546 ± 103	$+38$	283.7	282.6
	cold	-83 ± 7	-322 ± 25	-15	283.7	282.5
F31Y	heat	102 ± 8	302 ± 25	$+65$	284.9	283.2
	heat (400 MPa)	61 ± 5	171 ± 17	$+84$	285.3	283.3
	cold	-96 ± 22	-364 ± 80	-10	284.7	283.9

[a] Wild type at pH 7.4 in the presence of 4 M urea, F31A at pH 7.4, and F31Y at pH 3.

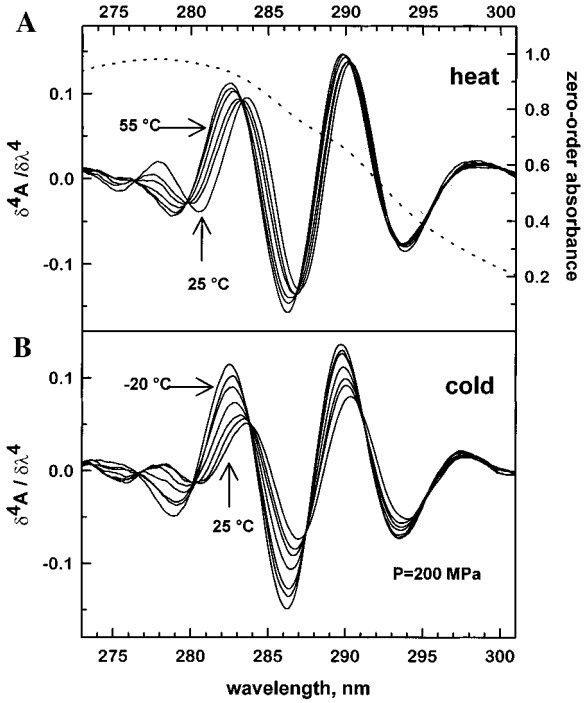

FIGURE 1: Fourth derivative UV spectra of F31A as a function of temperature: heat denaturation between 25 and 55 °C [the dotted line shows the zero-order spectrum at 30 °C (right-hand scale)] and cold denaturation between 25 and −20 °C; phosphate buffer, 50 mM, pH 7.4.

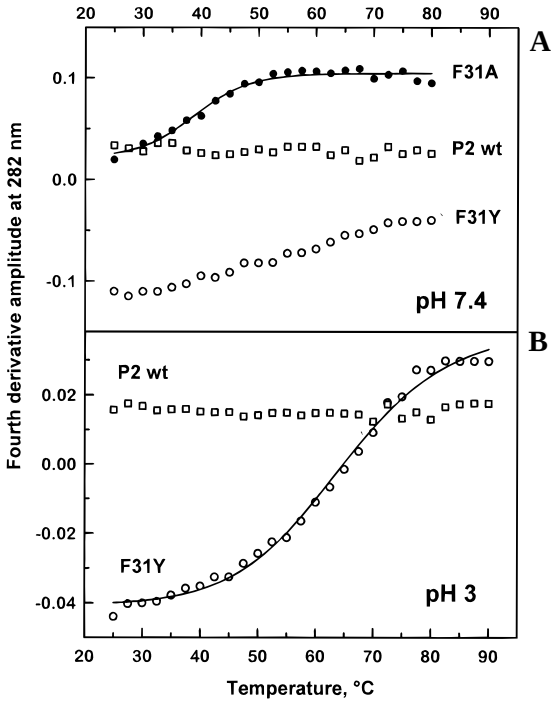

FIGURE 2: Heat denaturation profiles of wild-type P2 and its F31A and F31Y mutants. The fourth derivative amplitude at 282 nm was plotted as a function of temperature in phosphate buffer, 50 mM, pH 7.4, and pyrophosphate buffer, 50 mM, pH 3.0.

changes, which are difficult to analyze in the zero-order spectrum, become very clear in the fourth derivative mode. As shown in Figure 1A, heating the sample from 25 to 55 °C resulted in a blue shift of the characteristic tyrosine band from 283.7 nm, virtually identical to the wild type, to 282.6 nm, which is the same as for ATEE in water at 55 °C and indicates that the tyrosines become almost completely exposed to the solvent. This transition occurred with clear isosbestic points at 276.4, 279.8, and 283.2 nm, which allowed its treatment in terms of a simple two-state process. Taking the spectral amplitude at 282 nm (between the two main isosbestic points) as the signal for this process, a sigmoidal denaturation profile with a transition temperature of $t_m = 38$ °C was obtained (Figure 2A). Fitting eq 3 yielded the thermodynamic parameters $\Delta H = 170$ kJ/mol and $\Delta S = 546$ J/(mol·K). In addition, in the tryptophan region (near 290 nm) a small blue shift from 290.4 to 289.7 nm was also observed. However, the magnitude of this transition was too small to allow a quantification of the transition parameters.

Decreasing the temperature from 25 to −20 °C at 200 MPa resulted in a similar, but more pronounced, spectral transition. As shown in Figure 1B, both the characteristic tyrosine and tryptophan bands were blue shifted. The tyrosine band moved from $\lambda_{max} = 283.7$ to 282.5 nm, a larger shift than expected for ATEE under identical conditions, suggesting that the protein tyrosine environment is becoming more polar. In addition, the tryptophan band was shifted from 290.1 to 289.7 nm, indicating that the tryptophan environment also became more polar at low temperatures. Very clear isosbestic points characterized these spectral changes. In contrast to the denaturation by heat, the main isosbestic point of the tyrosine band appeared at 283.8 nm, which is 0.6 nm more to the red. Furthermore, the amplitude of the spectral changes was nearly twice that obtained by heat denaturation. From the denaturation profile of the amplitude in the tyrosine band, shown in Figure 3A, the thermodynamic parameters were determined as $\Delta H = -83$ kJ/mol, $\Delta S = -322$ J/(mol·K), and $t_m = -15.1$ °C. The denaturation profile in the tryptophan region did not result in significantly different parameters, suggesting that the tyrosine and tryptophan environments were affected in a cooperative way.

Applying pressure up to 400 MPa resulted again in a blue shift of the tyrosine band, with an isosbestic point at 283.5 nm. The tryptophan band was, however, not affected by pressure (see Figure 4A). From the pressure denaturation

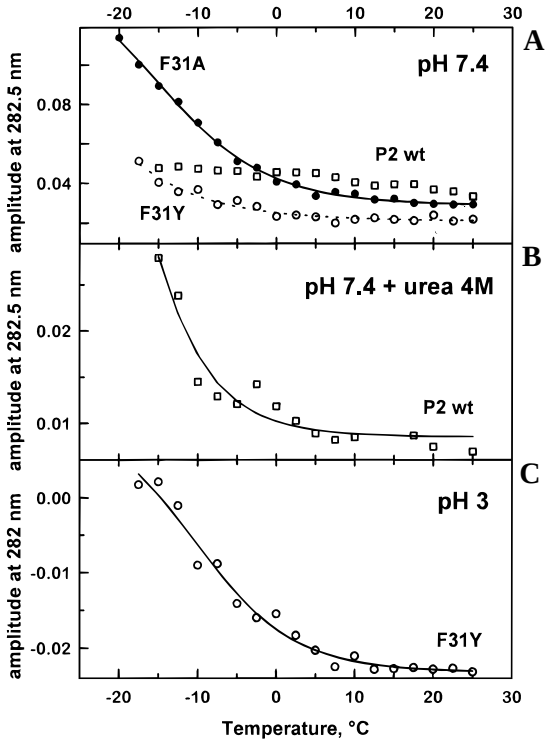

FIGURE 3: Cold denaturation profiles of wild-type P2 and its F31A and F31Y mutants: fourth derivative amplitude in the tyrosine region. Upper graph: phosphate buffer, 50 mM, pH 7.4 (the F31Y data were upshifted for a better comparison). Middle graph: same conditions but in the presence of urea, 4 M. Lower graph: pyrophosphate buffer, 50 mM, pH 3.

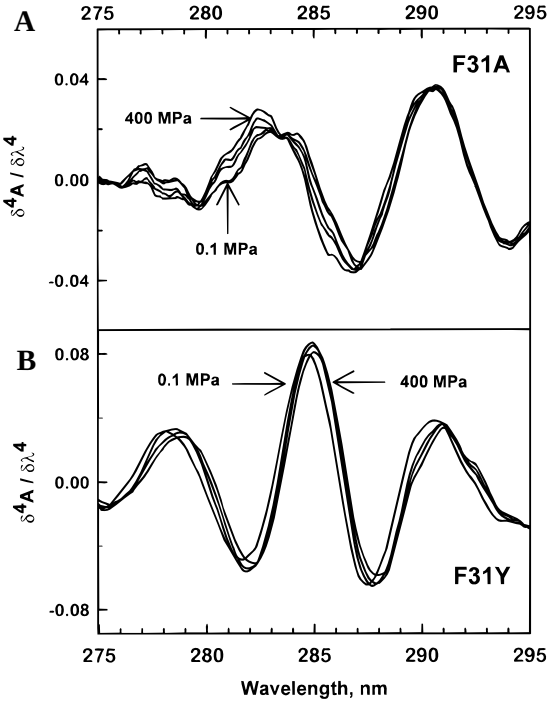

FIGURE 4: Fourth derivative spectral transitions of the F31A and F31Y mutants at high pressure: MES buffer, 50 mM at pH 5, T = 35 °C. The pressure was raised in steps of 50 MPa from room pressure to 450 MPa. Only a few spectra are shown. Note the pressure-induced blue shift in the upper graph and the red shift in the lower graph.

profile in Figure 5 the transition parameters were determined as $\Delta G_0 = 10.5$ kJ/mol and $\Delta V = -43$ mL/mol with a half-transition pressure of 256 MPa (see also Table 2).

Table 2: Thermodynamic Parameters of the Spectral Transition Induced by High Pressure at 35 °C and pH 5[a]

mutant	ΔV (mL/mol)	$\Delta G_{p=0}$ (kJ/mol)	p_m (MPa)	λ_m (nm) native at 0.1 MPa	λ_m (nm) denatured at 450 MPa
F31A	-43 ± 10	10.5 ± 2.2	256	283.5	282.6
F31Y	-23 ± 2	4.6 ± 0.3	200	284.7	285

[a] The experimental conditions were the same as those of Figure 5.

The F31Y Mutant. The introduction of a third tyrosine residue in place of Phe31 resulted in a spectral red shift of the tyrosine band to 284.9 nm at 25 °C, which corresponds to a mean dielectric constant of 38, indicating that the additional tyrosine is in a strongly hydrophobic environment. In addition, a new fourth derivative maximum appeared at 278.2 nm, which may arise from a tryptophan contribution which was masked by a spectral trough of the more polar (blue-shifted) tyrosines of the wild type and the F31A mutant. The F31Y mutant was rather stable at neutral pH, and a full high-temperature-induced spectral transition was obtained only at pH 3. Upon heating the sample to 90 °C, the wavelength maximum of the tyrosine band was blue shifted to 283.2 nm, converging on the value of 282.9 nm observed for ATEE in water at 90 °C. The spectrum at this temperature resembled that of the F31A mutant; i.e., the 278.2 band had disappeared. Again, the transition (t_m = 65 °C) was characterized by clear isosbestic points (276.2, 280.2, and 283.6 nm), and from the denaturation profile shown in Figure 2B the thermodynamic parameters could be evaluated as $\Delta H = 102$ kJ/mol and $\Delta S = 302$ J/(mol·K) (see also Table 2). The tryptophan band did not move as a function of temperature.

Under cold denaturation conditions the tyrosine, but not the tryptophan, component of the fourth derivative spectrum shifted slightly to the blue. Again, as shown in Figure 3A,C, the F31Y was more stable than the F31A mutant, and for an evaluation of the thermodynamic parameters the pH had to be lowered to pH 3. At this pH the tyrosine band of the derivative spectrum shifted from 284.7 to 283.9 nm. In contrast to the previous experiments, the isosbestic point was further to the red (284.4 nm) and rather noisy. The thermodynamic parameters are listed in Table 1.

Quite surprisingly, as shown in Figure 4B, an increase of pressure of up to 450 MPa resulted in a red shift of the fourth derivative spectrum: the tyrosine component was shifted from 284.7 to 285 nm. This indicates that at high pressure the tyrosines are in a less polar environment. This opposite effect of pressure on the tyrosine environment is illustrated in Figure 5, where the amplitude at the left-hand side of the derivative maximum in the tyrosine region is plotted as a function of pressure for the three proteins. From the sigmoidal shape of the transition the thermodynamic parameters could be evaluated as shown in Table 2.

A possible explanation for the observed red shift at high pressure is a closer interaction between the aromatic residues. If this is the case, high pressure would contribute to a higher stability of F31Y. To verify this hypothesis, we compared the high-temperature denaturation profiles of F31Y at atmospheric pressure and at 400 MPa. Indeed, as shown in Figure 6, high pressure protects the protein against denaturation by high temperature: the transition temperature was increased from 65 to 84 °C (see also Table 1).

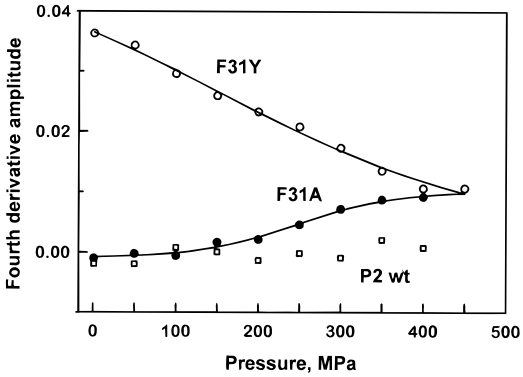

FIGURE 5: Spectral transition in the tyrosine region induced by high pressure. The transition was followed at a wavelength situated between the maximum of the tyrosine derivative peak and its adjacent blue-side trough where the amplitude of the changes had a maximum: at 281 nm for the wild type and F31A and at 283.6 nm for the F31Y. No spectral changes were observed for wild-type P2. For a comparison its derivative amplitude is shown at 281 nm. The experimental conditions were the same as those of Figure 4.

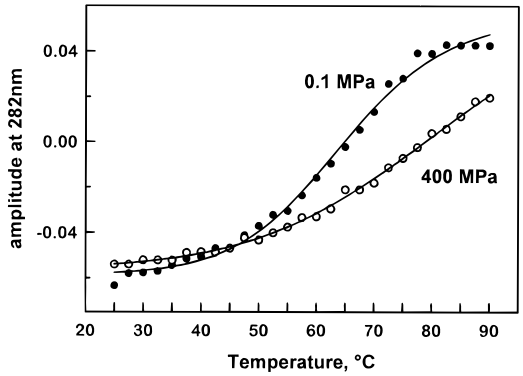

FIGURE 6: Heat denaturation profiles of the F31Y mutant at atmospheric pressure and at 400 MPa. The conditions were at atmospheric pressure, pyrophosphate buffer, 50 mM, pH 3, and at 400 MPa, phosphate buffer, 50 mM, pH 3. The pH had been corrected for pressure according to van Eldik et al. (1989).

Molecular Dynamics Simulation. In order to identify the core residues that contribute most to the stability of P2, we simulated a molecular dynamics trajectory of wild-type P2 with an explicit solvation scheme. In our calculations, the total energy and potential energy of the system were well conserved after equilibration (data not shown) and indicate the stability of the simulation. Loops interconnecting the secondary structures, and in particular residues 7−10, 35−40, and 61−63 (C-terminal), showed large root mean square (rms) deviations during the 410 ps of dynamics following an initial 40 ps equilibration. We calculated an average structure over 410 ps and compared it with the NMR average structure. The rms deviations between the NMR structure and our average structure are 1.62 Å for Cα atoms 1−59 (2.19 Å for all atoms). These values are smaller when restricting the comparison to the five β-sheet regions (respectively 1.06 Å for Cα and 1.87 Å for all atoms). Baumann et al. (1994) reported that the backbone conformation within the β-sheet regions was well defined, whereas the other regions, specially 35−40 and the C-terminal residues, were less well defined and showed a large degree of inherent flexibility. The general agreement between our simulation results and the NMR experimental data gave us added support to use our trajectory as a representative sample of the conformations explored by the protein on this time scale.

Using this trajectory, we calculated the contribution of each protein side chain to the total vdW energy term (Figure 7). The calculated values are a useful means of comparing relative vdW interaction energy of each residue with all the others. However, it should be stressed that the absolute values of the energy determined in this way are difficult to interpret and strongly depend on the parameters chosen for the simulation. The strongest interactions (colors red and yellow in Figure 7) were displayed by residues Phe5, Phe31, and Tyr33 throughout the 410 ps duration of the simulation. This confirms that the aromatic residues of the hydrophobic core make the major contribution to the overall vdW energy while the structure explores a conformational subspace. Tyr7 did not make a major contribution. Trp23, which is largely exposed to the solvent, made a significantly smaller contribution than Phe5, Phe31, and Tyr33, despite the fact that its large size favors the vdW energy term. The molecular dynamics simulation identifies, therefore, Phe31 as one of the most strongly interacting residues of the hydrophobic core.

DISCUSSION

Importance of the Hydrophobic Core Interactions. Probing the tyrosine environment, our results show an extreme stability of ribonuclease P2 toward temperature (from −20 to 90 °C) and pressure (at least up to 700 MPa). To our knowledge, no other protein has been described with such a wide range of stability. Analogous proteins isolated from other thermophilic archaebacteria, such as α-amylase from *Pyrococcus furiosus* (Laderman et al., 1993) or Sac7d from *Sulfolobus acidocaldarius* (Edmondson et al., 1995), are also highly thermostable, but there are as yet no pressure data available. However, when Phe31, which is one of the three residues of the hydrophobic core which has the strongest vdW interaction energy, is replaced by alanine or tyrosine, the stability of P2 becomes considerably lower. Hydrophobic interactions within the core appear, therefore, to be essential for maintaining the protein stability. In this respect, P2 behaves in a classical way—like mesophilic proteins. Indeed, one of the most important forces in protein folding is hydrophobic interaction—a concept which goes back to the work of Kauzmann (1959). A number of site directed mutagenesis experiments in which hydrophobic core residues are replaced by smaller ones have shown that loss of vdW contacts destabilizes proteins (Shortle et al., 1990; Buckle et al., 1996).

Complexity of the Denaturation Process. Whereas our results strongly suggest that the hydrophobic inner core interactions are essential for the stability of P2, the actual protein denaturation process appears to be more complex. Knapp et al. (1996), who studied recently the thermal unfolding of P2 by CD and differential scanning calorimetry (DSC), obtained evidence of a significantly lower thermal stability of P2. By these techniques, these authors obtained shallow transition curves under conditions where we did not see any change in the fourth derivative UV spectra. These different results are intriguing, since changes in ellipticity (from CD) and heat capacity (from DSC) inform potentially about structural changes of the peptide backbone chain, whereas our technique permits evaluation of the polarity

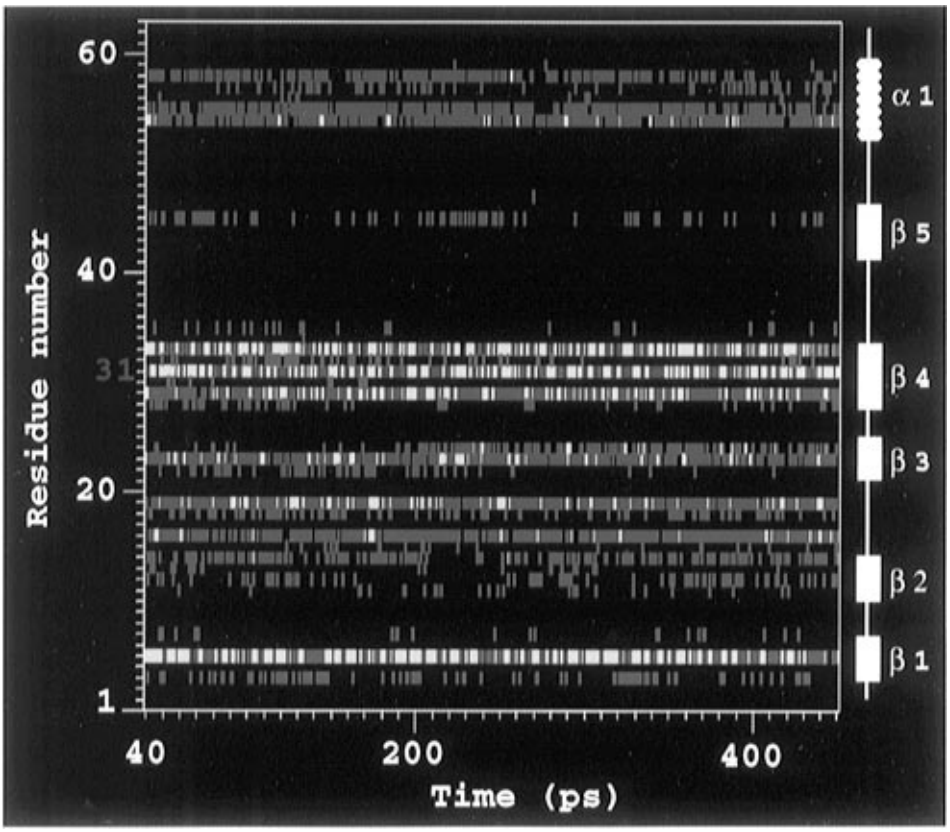

FIGURE 7: Van der Waals (vdW) energy contribution by each protein side chain during the dynamics simulation. VdW interaction energies of each side chain with the rest of the protein (*y* axis) are plotted as a function of simulation time. The secondary structure of the protein is represented schematically on the right. The energies are distributed between −12.7 and 11.6 kcal with an average of −3.5 kcal through the trajectory. Three low-energy levels (strong interaction) are indicated in color: between −12.7 and −10 kcal/mol, red; between −10 and −8 kcal/mol, yellow; and between −8 and −6 kcal/mol, green. Absence of color implies that, for this side chain at a given time, the vdW energy has a value greater than −6 kcal. The strongest interactions are displayed by the side chains of Phe5, Phe31, and Tyr33. Their relative contributions averaged over the simulation time are −8.5, −9.9, and −8.6 kcal, respectively. This figure was generated using SQUID (Oldfield, 1992).

changes (and thus the solvent exposure) of the Tyr33 environment (our molecular dynamics simulation indicated that Trp23 and Tyr7 are already significantly solvent exposed in the native state and in the calculated conformational subspace). The fact that this environment remains nonpolar until 90 °C, a temperature where the protein starts melting, suggests that the thermal denaturation of P2 occurs in several steps. The emerging picture is therefore that Phe5, Phe31, and Tyr33 belong to a hydrophobic solid-like domain which does not break at high temperature or high pressure. In contrast, the hydrophilic mantle would show increased flexibility and finally melt at higher temperature. Further support for this idea comes from the relatively large rms deviation of the backbone atoms of several outer parts of the protein during the dynamics simulation.

Aromatic Interactions. Among the hydrophobic forces, interaction between aromatic amino acids appears to be essential for maintaining the stability of P2. Indeed, the F31A mutant, which has lost the aromaticity at position 31, is much more sensitive to extreme conditions of temperature and pressure than the wild-type protein. Interestingly, for its heat denaturation process, the enthalpy change ΔH is very comparable to that obtained by DSC for the overall thermal unfolding of P2. This suggests that in the F31A mutant the stability of the hydrophobic domain is considerably weakened and its thermal solvent exposure is part of the protein unfolding process. The F31Y mutant, with a more polar but still aromatic residue at position 31, has a stability intermediate between the wild type and the F31A. The aromatic interactions thus appear to play a major role in stabilizing the tertiary structure of P2. This idea is strongly supported by the molecular dynamics simulation which shows that three aromatic residues (Phe5, Phe31, and Tyr33) exhibit the strongest vdW interaction energies throughout the trajectory. As shown in Figure 8, the aromatic rings of these residues lie nearly in one plane, but perpendicularly to that they form dihedral angles between 30° and 50°. This geometry is, however, not observed for the two other aromatic residues, Tyr7 and Trp23, which in addition appear to be rather exposed to water. In fact, aromatic interactions in this geometry are believed to stabilize the tertiary structure of many proteins—not only those from thermophilic organisms (Burley & Petsko, 1985). This feature seems to occur more frequently than a sandwich-like aromatic stacking (Dupureur et al., 1992). Thus, although this type of fishbone geometry of aromatic interactions certainly contributes to the stability of P2, this feature alone is not sufficient to explain the extreme stability of P2.

Structural Differences of Cold and Heat Denaturation. At low and high temperatures both mutants—the F31Y albeit to a lesser degree—underwent a structural change leading to a more polar mean environment of the tyrosines. From inspection of the structure and analysis of the dynamics simulation, we expect that in wild-type P2 Tyr7 would be significantly exposed to water. The same situation can be expected for the two mutants at room temperature, since their

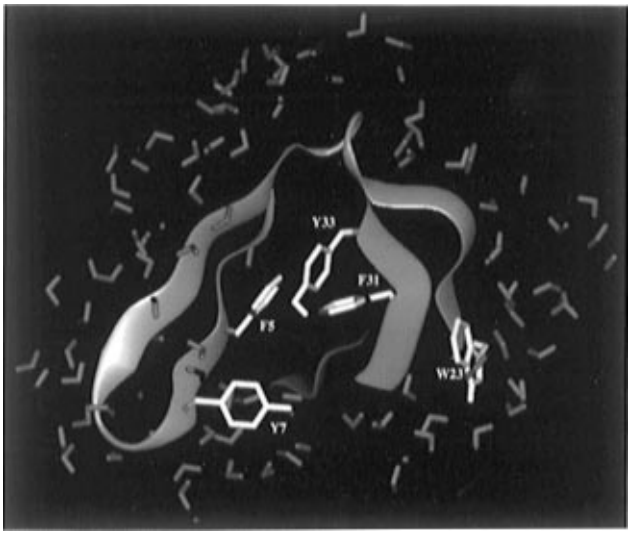

FIGURE 8: Ribbon diagram of the P2 structure model after solvation and equilibration. For clarity, the figure is limited to a thin depth slice of the core. The protein backbone (blue), all aromatic residues (yellow), and water molecules (red) that fall within 3 Å of the protein are represented. Hydrogens of the Tyr hydroxyl and the water molecules are included. The figure illustrates a distribution of water molecule packing around the protein. Note the accessibility of Tyr7 and Trp23 and the fishbone geometry of Phe5, Phe31, and Tyr33.

tertiary structures—as judged from NMR (Zetta et al., unpublished results) and from molecular dynamics simulation (Afshar et al., unpublished results)—appear to be nearly identical to wild-type P2. Our results with the mutants can therefore be explained by a cold- (and heat-) induced solvent exposure of Tyr33. The mechanism of the structural changes accompanying this increase in solvent exposure upon cold and heat denaturation is, however, not the same for the two processes. Although both denatured states were characterized by a very comparable increase of the mean polarity in the tyrosine environments, the isosbestic points of the spectral transition, as well as the energetic terms ΔH and ΔS of the reaction, were significantly different. A simple two-phase diagram employing a native and unique totally denatured state, as initially introduced by Hawley (1971) and used frequently up to now (Huang & Oas, 1996), is therefore not applicable for this protein. Instead, our results are closer to those of Zhang et al. (1995), Griko and Kutyshenko (1994), Konno et al. (1995), and Wong et al. (1996), who all found for a variety of proteins different features of heat and cold processes. Heat denaturation leads in most cases to a highly disordered protein structure. In contrast, the entropy-driven cold denaturation process leads generally to a protein state which contains still a significant amount of tertiary structure (Zhang et al., 1995; Konno et al., 1995; Foguel & Silva, 1994). Cold denaturation, which appears to be a common phenomenon for proteins (Franks et al., 1988), can be explained by a solvent exposure of hydrophobic residues where solvent water molecules are oriented to form an "ice-like" hydration shell (Dill, 1995). Similarly for P2, pressure and cold denaturation may result in intermediate states of protein unfolding, which could have the characteristics of molten globule or premolten globule states (Betz et al., 1996; Uversky & Ptitsyn, 1996).

Pressure-Induced Structural Changes. Most interestingly, at high pressures the polarity of the tyrosine environments increases for the F31A mutant and decreases for the F31Y mutant. A possible explanation for the F31A mutant would be that the replacement of Phe31 by alanine generates a nonpolar cavity which could be partially filled with water under high pressure (Prevelige et al., 1994). Currently, we are carrying out a molecular dynamics simulation of the mutants in order to verify this hypothesis. Alternatively, the denaturation by pressure may be explained by the fact that the former stabilizing aromatic network is weakened by the absence of Phe31. In contrast, the F31Y mutant has probably still an effective—although not optimal—aromatic interaction. Its pressure-induced spectral red shift can therefore be understood as an increased aromatic interaction between Tyr33, Phe5, and the new Tyr31. Indeed, aromatic interactions are thought to be strengthened by pressure (Scarlata, 1991; Weber & Drickamer, 1983; Mozhaev et al., 1996). A pressure-induced strengthening of these aromatic interactions thus possibly explains also why pressure protects the F31Y mutant against thermal denaturation. Similar protective effects of pressure have been observed in other proteins from thermophilic organisms (Mombelli et al., 1996; Hei & Clark, 1994).

Structural Basis of the Stability of P2. It is clear now that the factors commonly associated with protein stability, i.e., hydrogen bonding, salt bridges, absence of cavities (Eijsink et al., 1992), abundance of prolines (Kitakuni et al., 1994), or disulfide bridges, are not implicated in the structural stability of P2. In contrast, the hydrophobic domain containing in its center three aromatic residues disposed in a fishbone geometry contributes strongly to the protein stability. This type of interaction may lead to lower the conformational flexibility of this domain, which in turn could be related to the protein's thermal stability (Wüthrich et al., 1980; Anderson et al., 1993; Feller et al., 1994).

As discussed above, this cannot be the only structural feature responsible for its thermo- and barostability. The noncooperativity between the solvent exposure of the hydrophobic core compared with the unfolding of the peptide chain, as well as the shallow thermal unfolding profile (Knapp et al., 1996), has to be reconciled. It is likely that there is a multistage denaturation process in which the flexibility of the polypeptide chain in the hydrophilic mantle increases steadily while the hydrophobic core remains intact, even under extreme conditions of temperature and pressure, and prevents a total (irreversible) unfolding of the protein. In agreement with Knapp et al. (1996), this explanation of the stability of P2 is thus a combination of a complex thermodynamic unfolding process together with the presence of a small, very stable hydrophobic domain. Our hypothesis is consistent with the finding that when the stability of the hydrophobic domain is weakened—as in the case of the mutants—the thermal denaturation profile of the hydrophobic core—as sensed by our method—is also rather shallow, comparable to the global denaturation profile of the wild type observed by Knapp et al. (1996). It is therefore likely that the denaturation of the hydrophobic core of the mutants is a concerted process with peripheral protein parts. It could be that the structural connection between the hydrophobic domain and the more temperature sensitive remainder of the protein depends on the singular β-sheet structure of P2. Interestingly, the cold-shock protein CS7.4, which is rather stable to heat denaturation, is also largely in a β-sheet conformation (Chatterjee et al., 1993).

At present we can only speculate whether our explanation could be generalized for other thermo- and barostable proteins. For instance, Eijsink et al. (1995), working with thermolysin-like proteinase, did not observe a significant effect upon mutations in the hydrophobic core of the protein. However, the important region turned out to be a solvent-exposed part of the N-terminal part. Furthermore, Macedo-Ribeiro et al. (1996), who compared the thermostability of ferredoxin from thermophilic and mesophilic organisms, did not find large changes in the overall structure but many small changes which all could contribute to a decreased flexibility of the thermophilic protein. So it may be that different classes of thermophilic proteins cope with the potentially adverse high-temperature and pressure conditions by different mechanisms.

Conclusion. In this study the heat, cold, and pressure denaturation profiles of a hydrophobic domain of a thermophilic protein and its mutants are determined for the first time. Our results suggest a stabilizing mechanism where the protein maintains its characteristics at extreme conditions of temperature and pressure by a combination of complex unfolding thermodynamics of peripheral protein regions while maintaining a particularly stable small hydrophobic domain. The precise structural integrity required to be preserved under extreme conditions may be largely determined by the function of the protein. This could explain the diversity of stabilizing features in the various extremophilic proteins reported so far and provide insight into the more general principles connecting protein stability, architecture, and function. To study the stabilization mechanism further, kinetic studies are needed to establish the sequence and transition states of structural changes and compare with those of other proteins (Gas et al., 1993; Shaw & Bott, 1996; Foguel et al., 1995). In these experiments it would be interesting to investigate the behavior of different protein classes (TIM barrel, IgG, lipases, etc.) and establish whether each class shares any of the folding/unfolding characteristics. Furthermore, simulations of P2 and its two mutants, F31Y and F31A, by molecular dynamics at high temperature and pressure should provide a molecular basis for elucidating the structural changes involved. The details of current simulations will be discussed elsewhere.

ACKNOWLEDGMENT

We are grateful to Dr. C. Verma for help with the simulations, to Prof. Guy Dodson for critical reading of and comments on the manuscript, and to Dr. C. Balny for stimulating discussions.

REFERENCES

Anderson, D. E., Hurley, J. H., Nicholson, H., Baase, W. A., & Matthews, B. W. (1993) *Protein Sci. 2*, 1285−1290.

Baumann, H., Knapp, S., Lundbäck, T., Ladenstein, R., & Härd, T. (1994) *Nat. Struct. Biol. 1*, 808−819.

Bernstein, F., Koetzle, T., Williams, G., Meyer, J., Brice, M., Rodgers, J., Kennard, O., Shimanouchi, T., & Tasumi, M. (1977) *J. Mol. Biol. 112*, 535−542.

Betz, S. F., Raleigh, D. P., DeGrado, W. F., Lovejoy, B., Anderson, D., Ogihara, N., & Eisenberg, D. (1996) *Folding Des. 1*, 57−64.

Brooks, B. R., Bruccoleri, R. E., Olafsen, B. D., States, D. J., Swanimathan, S., & Karplus, M. (1983) *J. Comput. Chem. 4*, 187−217.

Brooks, C. L., III, & Karplus, M. (1989) *J. Mol. Biol. 208*, 159−181.

Buckle, A. M., Cramer, P., & Fersht, A. R. (1996) *Biochemistry 35*, 4298−4305.

Burley, S. K., & Petsko, G. A. (1985) *Science 229*, 23−28.

Caflisch, A., & Karplus, M. (1995) *J. Mol. Biol. 252*, 672−708.

Chatterjee, S., Jiang, W., Emerson, S. D., & Inouye, M. (1993) *J. Biochem. (Tokyo) 114*, 663−669.

Consonni, R., Fusi, P., Goossens, K., Grisa, M., Heremans, K., Puricelli, P., Tortora, P., Vanoni, M., & Zetta, L. (1996) in *High Pressure Bio-Science and Bio-Technology* (Heremans, K., Ed.) pp 31−34, Leuven University Press, Leuven, Belgium.

De Rosa, M., Gambacorta, A., Nicolaus, B., Giardina, P., Poerio, E., & Buonocuore, V. (1984) *Biochem. J. 224*, 407−414.

Dill, K. A. (1990) *Biochemistry 29*, 7133−7155.

Dupureur, C. M., Yu, B. Z., Mamone, J. A., Jain, M. K., & Tsai, M. D. (1992) *Biochemistry 31*, 10576−10583.

Edmondson, S. P., Quiu, L., & Shriver, J. W. (1995) *Biochemistry 34*, 13289−13304.

Eijsink, V. G. H., Dijkstra, B. W., Vriend, G., van der Zee, J. R., Veltman, O. R., van der Vinne, B., van der Burg, B., Kempe, S., & Venema, G. (1992) *Protein Eng. 5*, 421−426.

Eijsink, V. G. H., Veltman, O. R., Aukema, W., Vriend, G., & Venema, G. (1995) *Nat. Struct. Biol. 2*, 374−379.

Fasman, G. D. (1976) in *Handbook of biochemistry and molecular biology*, 3rd ed., Vol. 1, CRC Press, Inc., Cleveland, OH.

Feller, G., Payan, F., Theys, F., Qian, M., Haser, R., & Gerday, C. (1994) *Eur. J. Biochem. 222*, 441−447.

Foguel, D., & Silva, J. L. (1994) *Proc. Natl. Acad. Sci. U.S.A. 91*, 8244−8247.

Foguel, D., Teschke, C. M., Prevelige, P. E., Jr., & Silva, J. L. (1995) *Biochemistry 34*, 1120−1126.

Franks, F., Hatley, R. H., & Friedman, H. L. (1988) *Biophys. Chem. 31*, 307−315.

Fusi, P., Tedeschi, G., Aliverti, A., Ronchi, S., Tortora, P., & Guerritore, A. (1993) *Eur. J. Biochem. 211*, 305−310.

Fusi, P., Grisa, M., Mombelli, E., Consonni, R., Tortora, P., & Vanoni, M. (1995) *Gene 154*, 97−102.

Gast, K., Damaschun, G., Damaschun, H., Misselwitz, R., & Zirwer, D. (1993) *Biochemistry 32*, 7747−7752.

Gibson, R. E., & Loeffler, O. H. (1941) *J. Am. Chem. Soc. 63*, 898−906.

Griko, Y. V., & Kutyshenko, V. P. (1994) *Biophys. J. 67*, 356−363.

Hawley, S. A. (1971) *Biochemistry 10*, 2436−2442.

Hei, D. J., & Clark, D. S. (1994) *Appl. Environ. Microbiol. 60*, 932−939.

Herbert, R. A. (1992) *TIBTECH 10*, 395−402.

Huang, G. S., & Oas, T. G. (1996) *Biochemistry 35*, 6173−6180.

Hui Bon Hoa, G., Douzou, P., Dahan, N., & Balny, C. (1982) *Anal. Biochem. 120*, 125−135.

Jorgensen, W. L., Impey, R. W., Chandrasekhar, J., Madura, J. D., & Klein, M. L. (1983*) J. Chem. Phys. 79*, 926−935.

Kauzmann, W. (1959) *Adv. Protein Chem. 14*, 1.

Kell, G. S. (1973) in *Handbook of Chemistry and Physics* (Weast, R. C., Ed.) 54 ed., p F5, Chemical Rubber Publishing Co., Cleveland, OH.

Kitakuni, E., Kuroda, Y., Oobatake, M., Tanaka, T., & Nakamura, H. (1994) *Protein Sci. 3*, 831−837.

Kitamura Y., & Itoh, T. (1987) *J. Solution Chem. 16*, 715−725.

Knapp, S., Karshikoff, A., Berndt, K. D., Christova, P., Atanasov, B., & Ladenstein, R. (1996) *J. Mol. Biol. 264*, 1132−1144.

Konno, T., Kataoka, M., Kamatari, Y., Kanaori, K., Nosaka, A., & Akasaka, K. (1995) *J. Mol. Biol. 251*, 95−103.

Laderman, K. A., Davis, B. R., Krutzsch, H. C., Lewis, M. S., Griko, Y. V., Privalov, P. L., & Anfinsen, C. B. (1993) *J. Biol. Chem. 268*, 24394−24401.

Lange, R., Frank, J., Saldana, J. L., & Balny C. (1996a) *Eur. Biophys. J. 24*, 277−283.

Lange, R., Bec, N., Mozhaev, V. V., & Frank, J. (1996b) *Eur. Biophys. J. 24*, 284−292.

Lange, R., Bec, N., Frank, J., & Balny, C. (1996c) in *High Pressure Bioscience and Biotechnology* (Hayashi, R., & Balny, C., Eds.) pp 135−140, Elsevier Science B.V., Amsterdam.

Macedo-Ribeiro, S., Darimont, B., Sterner, R., & Huber, R. (1996) *Structure 4*, 1291−1301.

Mombelli, E., Bec, N., Tortora, P., Balny, C., & Lange, R. (1996) *Food Biotechnol. 10,* 131−142.
Mozhaev, V. V., Heremans, K., Frank, J., Masson, P., & Balny, C. (1996) *Proteins 24,* 81−91.
Mozo-Villarias, A., Morros, A., & Andreu, J. M. (1991) *Eur. Biophys. J. 19,* 295−300.
Oldfield, T. (1992) *J. Mol. Graphics 10,* 247−252.
Prevelige, P. E., Jr., King, J., & Silva, J. L. (1994) *Biophys. J. 66,* 1631−1641.
Scarlata, S. F. (1991) *Biochemistry 30,* 9853−9859.
Shaw, A., & Bott, R. (1996) *Curr. Opin. Struct. Biol. 6,* 546−550.
Shortle, D., Stites, W. E., & Meeker A. K. (1990) *Biochemistry 29,* 8033−8041.
Uversky, V. N., & Ptitsyn, O. B. (1996) *J. Mol. Biol. 255,* 215−228.
Van Eldik, R., Asano, T., & Le Noble, W. J. (1989) *Chem. Rev. 89,* 549−688.
Weber, G., & Drickamer, H. G. (1983) *Q. Rev. Biophys. 16,* 89−112.
Wong, K. B., Freund, S. M. V., & Fersht, A. R. (1996) *J. Mol. Biol. 259,* 805−818.
Wroblowski, B., Diaz, J. F., Heremans, K., & Engelborghs, Y. (1996) *Proteins 25,* 446−455.
Wüthrich, K., Wagner, G., Richarz, R., & Braun, W. (1980) *Biophys. J. 32,* 549−560.
Zhang, J., Peng, X., Jonas, A., & Jonas, J. (1995) *Biochemistry 34,* 8631−8641.

BI970467V